

The oral presentation of the material will take place at 18:00 CEST. If you are interested in, please attend a related Zoom meeting (see <https://drive.google.com/file/d/1k2uHDQnWPIHES3hXfKiy8VEYYFfyhM-8/view>).

ResearchGate

See discussions, stats, and author profiles for this publication at: <https://www.researchgate.net/publication/332333335>

# Quasi-stationary Current Sheets of the Solar Origin in the Heliosphere

Article in The Astrophysical Journal · April 2019

DOI: 10.3847/1538-4357/ab0dff

CITATIONS

2

READS

63

3 authors:



Roman Anatolevich Kislov

Space Research Institute

19 PUBLICATIONS 32 CITATIONS

SEE PROFILE



Olga V. Khabarova

Pushkov Institute of Terrestrial Magnetism, Ionosphere and Radio Wave Propagati...

85 PUBLICATIONS 762 CITATIONS

SEE PROFILE



H. V. Malova

Lomonosov Moscow State University

183 PUBLICATIONS 2,000 CITATIONS

SEE PROFILE

Some of the authors of this publication are also working on these related projects:






Russian-French project of the Russian Foundation for Basic Research "Current sheets and plasma dynamics in 3D structures near magnetic separatrixes [View project](#)



Heavy ions [View project](#)

# Quasi-stationary Current Sheets of the Solar Origin in the Heliosphere

Roman A. Kislov<sup>1,2</sup> , Olga V. Khabarova<sup>2</sup> , and Helmi V. Malova<sup>1,3</sup> 

<sup>1</sup> Space Research Institute of Russian Academy of Sciences (IKI RAS), Moscow, 117997, Russia

<sup>2</sup> Pushkov Institute of Terrestrial Magnetism, Ionosphere and Radio Wave Propagation, Russian Academy of Sciences, Troitsk, Moscow, 108840, Russia

<sup>3</sup> Scobeltsyn Nuclear Physics Institute of Lomonosov Moscow State University, Moscow, 119991, Russia

## Abstract

The solar magnetic field (SMF) has historically been considered as dipole in order to build models of the radially expanding corona, that is, the solar wind in the solar minimum. The simplified approach suggests the existence of only one quasi-stationary current sheet (QCS) of solar origin in the heliosphere, namely, the heliospheric current sheet (HCS). However, the SMF becomes more complicated over the solar cycle, comprising higher-order components. The overlapping of the dipole and multipole components of the SMF suggests a formation of more than one QCS in the corona, which may expand further to the heliosphere. We study the impact of the quadrupole and octupole harmonics of the SMF on the formation and spatial characteristics of QCSs, building a stationary axisymmetric MHD model of QCSs in the heliosphere. It is shown that if the dipole component dominates, a single QCS appears in the solar wind at low heliolatitudes as the classic HCS. In other cases, the number of QCSs varies from one to three, depending on the relative input of the quadrupole and octupole components. QCSs possess a conic form and may occur at a wide variety of heliolatitudes. The existence of QCSs opens wide opportunities for explanations of puzzling observations of cosmic rays and energetic particles in the heliosphere and, at the same time, raises a risk of misinterpretation of in situ crossings of QCSs because of mixing up the HCS and higher-heliolatitude QCSs, which can be significantly disturbed in the dynamical solar wind.

**Key words:** solar wind – Sun: heliosphere – Sun: magnetic fields

## 1. Introduction

The existence of at least one long-lived stable current sheet in the heliosphere is an observational fact, confirmed by numerous in situ measurements of the interplanetary magnetic field (IMF). The heliospheric current sheet (HCS) separating oppositely directed IMF lines was discovered many years ago and still remains the best-known structure carrying the electric current in the solar wind (Davis 1965; Wilcox & Ness 1965; Wilcox 1968; Svalgaard & Wilcox 1975; Bruno et al. 1982). A detailed analysis of HCS crossings shows that the HCS is embedded into a much wider heliospheric plasma sheet (HPS) (Winterhalter et al. 1994; Bavassano et al. 1997; Crooker et al. 2004; Suess et al. 2009; Simunac et al. 2012; Khabarova et al. 2015, 2017b). Both the HPS and the HCS possess a fine structure, reproducing themselves at higher scales, similarly to all strong current sheets (SCSs) in the heliosphere and magnetosphere (Malova et al. 2017, 2018). Under a rough approximation, the HCS–HPS system can be considered as a unified magnetic separator, which is called a sector boundary.

Historically, attempts to describe the HCS theoretically were based on the understanding of the fact that the magnetic field of the quiet Sun can be approximately be described as dipole. Therefore, if there are two hemispheres (or sectors) with the oppositely directed magnetic field, there should be a magnetic separator between them representing a neutral line at the Sun and a sheet in the solar wind (Davis 1965; Wilcox & Ness 1965; Wilcox 1968; Alfvén 1977, 1981; Nerney et al. 1995; Fisk 1996; Veselovsky et al. 2002; Schwadron & McComas 2005; Czechowski et al. 2010; Usmanov et al. 2012). A solar origin of the IMF sector structure became evident from the very beginning of the space era (Ness & Wilcox 1964). A neutral surface of the HCS was thought to represent an extension of the solar magnetic field (SMF) equator to the heliosphere (Antonucci & Svalgaard 1974). In

the meantime, a direct association between the position of the neutral line on the Sun and the position of the HCS in the heliosphere should be considered with some caution, as attempts to associate HCS crossings with a radial projection of the magnetic equator line into the solar wind have not been quite successful (e.g., Behannon et al. 1981).

Historically, the existence of the quadrupole magnetic field was thought to be responsible for observations of four sectors of the IMF at 1 au (Schultz 1973; Girish & Prabhakaran Nayar 1988), although it was also shown that a wavy form of the solar magnetic equator might produce the same observational effect (Svalgaard et al. 1974). The latter generally correlated with observations better (Korzhov 1977) and became a dominant paradigm within which IMF lines could be traced/mapped back to the corona or, to be exact, to the source surface. The source surface is defined as an empirically set sphere, below which magnetic field lines are closed and above which they are radially open (Schatten et al. 1969). The introduction of the source surface has allowed the creation of successful semiempirical models (i.e., Wang & Sheeley 1990). However, this method has some limitations because the boundary of the solar atmosphere is actually defined by the Alfvén surface of a nonspherical and variable shape. It changes with changing solar activity, represents a broad area, and cannot be indicated precisely as a sphere located at some certain distance from the Sun (Cohen 2015; DeForest et al. 2018). Attempts to find solutions for the key solar wind parameters also face a problem as those may have discontinuities at the Alfvén surface. As a result, it is difficult to reconstruct full maps of magnetic fields, the speed, and the plasma concentration near the Sun correctly (Vlahakis et al. 2000). An additional problem arises from the strong spatial and temporal variability of the SMF and the short-term effects of the solar activity (Hale et al. 1919; Parker 1958, 1969). As a

result, modeling of the large-scale structure of the expanding solar wind is still an actively developing area of plasma physics because of the great uncertainty in choosing boundary conditions.

If the SMF possesses higher harmonics in addition to the main dipole, more magnetic structures can appear in the solar wind owing to overlapping of the dipole with the quadrupole, the octupole, and so on. The quadrupole component is significant and cannot be neglected, for example, during periods of high solar activity (Sanderson et al. 2003). Higher-order components of the magnetic field, such as the octupole component, can also appear in the course of a solar cycle, which complicates the entire picture of the SMF and its extension into the heliosphere considerably (Obridko & Shelting 2008; DeRosa et al. 2012; Obridko et al. 2012). The overlapping of the dipole and higher-order components of the SMF results in the formation of magnetic separators or neutral lines at different scales at the Sun (Edmondson et al. 2010; Titov et al. 2012; Higginson et al. 2017). It is natural to suggest that some of those neutral lines extend to the expanding solar wind and form quasi-stationary current sheets (QCSs) similar to the HCS. It is also reasonable to suggest that in contrast to relatively small-scale neutral lines occurring between active regions of different polarities, neutral lines formed by overlapping dipole and higher harmonics of the SMF should be the most stable structures and can be considered as potential sources of QCSs in the solar wind. There are very few studies on the stability of current sheets in the heliosphere, including the HCS (see, e.g., Dobrowolny & Trussoni 1979). The HCS has been supposed to be very stable just because it definitely exists and is observable through the entire space era. The paradox is that simple estimations show that thin current sheets of the Harris type should be extremely sensitive to a tearing mode and, consequently, very unstable (Coppi et al. 1966; Dobrowolny & Trussoni 1979). This paradox has been solved in magnetospheric physics. Lembege & Pellat (1982), and later Zelenyi et al. (2008), showed that the vertical component of the magnetic field stabilizes current sheets significantly. Since this condition is always realized in the solar wind, if a current sheet is formed in the solar atmosphere and strong enough to survive up to the source surface, it possesses all properties of the HCS, including its stability. Furthermore, an analysis of the fine structure of SCSs in the heliosphere shows that an SCS represents a complex system of currents flowing in one direction (Malova et al. 2017, 2018). As a result, the attraction of undirected currents suppresses the development of instabilities in the current sheet, allowing it to extend to large distances.

The fact that the HCS is not the only large-scale and long-lived current sheet in the solar wind has recently been confirmed by observations of long-lived conic current sheets located inside polar coronal holes. These structures of a conic form have been found in the corona and in situ at several heliocentric distances (Khabarova et al. 2017a). The conic neutral surfaces can be interpreted as extensions of closed local neutral lines formed in polar regions of the Sun as a result of the overlapping dipole and quadrupole. This finding supports an idea of the existence of more than one current sheet in the solar wind and stimulates us to develop a model of QCSs in the heliosphere that takes into account the nondipole nature of the SMF. Furthermore, it has been confirmed that the found polar conic current sheets serve as channels for energetic particles,

which is a quite natural and well-known feature of current sheets. Therefore, if there are more current sheets at high heliolatitudes, this will offer an opportunity to reconsider possible ways of global propagation of energetic particles in the heliosphere.

As mentioned above, a single magnetic separator appears naturally in all simplified models of the solar wind with the dipole magnetic field. The present study is not aimed at the modeling of the entire solar wind, but rather at the creation of a model that describes the appearance and spatial profiles of stationary current sheets that are determined by the real structure of the SMF, which is more complex than a simple dipole. We develop a one-fluid MHD model of the IMF, considering the quadrupole and octupole SMF components as possible sources of additional current sheets comparable to the HCS by scale and strength. Within the model, stationary solutions corresponding to the existence of QCSs are found. We show that from one to three current sheets can be formed in the solar wind, depending on the contribution of quadrupole and octupole components to the total SMF.

## 2. Current Sheets in the Heliosphere Formed by a Superposition of the Dipole and Multipole Magnetic Fields of the Sun

To build a model of QCSs in the solar wind, we need to show from the very beginning a possibility of the existence of multiple current sheets near the Sun. Below we set a randomly chosen sphere around the Sun and consider the axisymmetric dependence of the magnetic flux on latitude at the sphere. In the case of overlapped magnetic fields of the dipole, the quadrupole, and the octupole, more than one neutral line may occur at the sphere. Since the solar wind expands, the lines become surfaces, extending to rather far heliocentric distances. At this stage, questions on the modeling of the form, position, and evolution of the resulting neutral surfaces/current sheets as well as their stability arise. In the current study, we will solve a set of the former problems, not discussing the stability of formed current sheets (see the corresponding discussion in the introduction). We will illustrate a potential opportunity of the formation of QCSs in the heliosphere, in addition to the well-known HCS.

### 2.1. Neutral Magnetic Field Lines on the Sun in the Case of the Overlapping Dipole and Quadrupole Magnetic Fields

We will consider below a simplified case of the axisymmetric SMF. A cylindrical coordinate system  $(r, \varphi, z)$  with the beginning in the center of the Sun is employed in which the  $z$ -axis is directed along the axis of symmetry of the magnetic field as shown in Figure 1. Since the task requires a setting of the magnetic flux at an arbitrary sphere around the Sun, we also employ a spherical system of coordinates  $(R, \theta, \varphi)$ , where  $\theta$  is the angle between the north pole and a chosen direction.

We will follow a standard magnetic flux method employed by Kislov et al. (2015), assuming that two of the three magnetic field components can be determined in terms of magnetic flux derivatives, which automatically ensures that the magnetic field is nondivergent:

$$B_r = -\frac{\partial \Phi}{r \partial z} \quad (1)$$

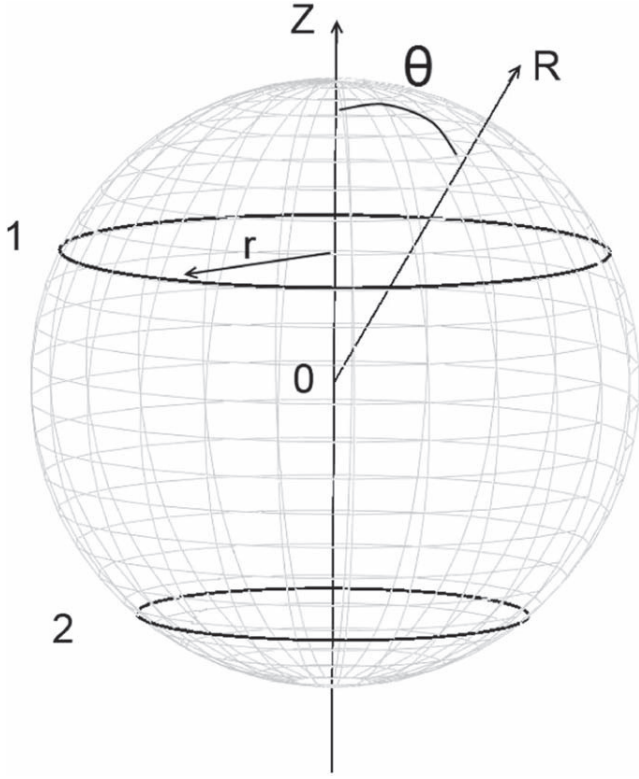


**Figure 1.** System of coordinates employed in the model;  $r$  is the cylindrical radius. Spherical radius is denoted as  $R$ ,  $z$  is the axis of rotation, and  $\theta$  is the polar angle. Zero is the center of coordinates. Circles 1 and 2 on the sphere illustrate possible positions of neutral lines of the SMF near the Sun in the case of the mixed “dipole-quadrupole” magnetic field with quadrupolarity  $\varepsilon = 2$  (see below).

$$B_z = \frac{\partial \Phi}{r \partial r}. \quad (2)$$

In the configuration examined here, the total magnetic field comprises both a magnetic dipole and a magnetic quadrupole with the axes of symmetry parallel to each other and  $z$ . The tensor of the magnetic quadrupole moment is diagonal in the chosen coordinate system. The magnetic flux on the surface between the north pole and a chosen direction of  $\theta$  is

$$\Phi = \Phi_0 \sin^2 \theta (1 + \varepsilon \cos \theta), \quad (3)$$

where  $\Phi_0 \sin^2 \theta$  is the magnetic flux of the dipole,  $\varepsilon \Phi_0 \sin^2 \theta \cos \theta$  is the magnetic flux of the quadrupole,  $\Phi_0 = \mu/R_0$ ,  $\mu$  is the dipole magnetic moment of the Sun, and  $R_0$  indicates the radius of the arbitrary sphere. Here,  $\varepsilon$  is a ratio of amplitudes of the quadrupole magnetic flux to the dipole magnetic flux called a quadrupolarity rate.

As a result of the superposition of the dipole and the quadrupole, neutral surfaces appear. The position of a neutral surface is determined by the latitudinal extremum of the magnetic flux. It is easy to find that extremes of  $\Phi$  in Equation (3) have the following view:

$$\cos \theta = \frac{-1 \pm \sqrt{1 + 3\varepsilon^2}}{3\varepsilon}. \quad (4)$$

According to Equation (4), neutral surfaces possess a conic shape with the  $2\theta$  cone angle. At  $\varepsilon \rightarrow 0$ , that is, in the dipole

magnetic field limit, only one extremum exists, which has the equatorial position ( $\cos \theta = 0$ ) and corresponds to expectations of Parker-like models to observe only one current sheet, namely, the HCS, at low heliolatitudes in solar minimum. Meantime, increasing  $\varepsilon$  leads to a northward shift of the position of a neutral surface, and if  $\varepsilon$  decreases, a southward shift takes place. At  $\varepsilon = 1$ , a second extremum at the south pole appears. If  $|\varepsilon|$  keeps growing, the location of the second neutral line on the arbitrary surface around the Sun moves toward the equator.

In the limit case of  $\varepsilon \rightarrow 8$ , that is, if there is the quadrupole magnetic field only, the initial neutral line position rises up to  $\cos \theta = 1/\sqrt{3}$  (i.e.,  $\theta = 55^\circ$ ), and the second extremum moves to the equatorial line position (to  $\cos \theta = -1/\sqrt{3}$ ). At negative  $\varepsilon$ , a resulting configuration and corresponding changes are symmetric to those described above, that is, an additional extremum appears at the north pole and moves toward the equator under growing large absolute values of negative  $\varepsilon$ .

Figure 2(a) shows the dependence in Equation (4). The vertical axis reflects the  $\theta/\pi$  angle, and the horizontal axis stands for  $\varepsilon$ . The red curve corresponds to the solutions of Equation (4) calculated for the positive sign, and the blue curves show the same for the negative sign. One can see that the solutions for the negative sign do not exist in every case, but only if  $|\varepsilon| > 1$ . These solutions correspond to the occurrence of an additional high-latitude neutral line. Different values of  $\varepsilon$  obviously reflect different phases of solar activity, as the dipole-to-quadrupole ratio changes over solar cycle (Obridko et al. 2012; Wang 2014). For example, one can suggest that the picture of neutral lines at  $\varepsilon \rightarrow 0$  corresponds to solar minimum, and  $\varepsilon \rightarrow 8$  corresponds to the period of the polarity reversal.

Summarizing, in the case of the overlapping dipole and quadrupole magnetic fields of the Sun, either one or two QCSs can exist in the solar wind.

## 2.2. Neutral Lines on the Sun in the Case of the Existing Octupole Magnetic Field

We have shown above that even a very simple consideration of the overlapping dipole-quadrupole SMFs suggests the existence of more than one stable neutral line at the Sun. Furthermore, Figure 2 reveals the fact that if two neutral lines appear, these are located above the equator.

It should be noted that 3D reconstructions of the IMF and the solar wind speed structure based on interplanetary scintillation measurements show that, independently of solar cycle and original location of the magnetic equator on the Sun, there is a QCS at relatively low heliolatitudes, which is considered to be the HCS (see [http://smei.ucsd.edu/new\\_smei/data&images/data&images.html](http://smei.ucsd.edu/new_smei/data&images/data&images.html), and Bisi et al. 2008; Bisi 2016; Jackson et al. 2004, 2006, 2008, 2009; Khabarova et al. 2015, 2016). The interplanetary scintillation reconstructions suggest that although the HCS form quickly varies in accordance with variable conditions of the interplanetary medium and may even break down into many leaf-like current sheets, the HCS has a tendency toward restoration in the form of a smoothly wavy structure under quiet conditions. This means (1) that a form of the magnetic equator at the Sun (which can sometimes reach high latitudes) does not completely determine a form of the HCS in the solar wind and (2) the presence of the HCS at low



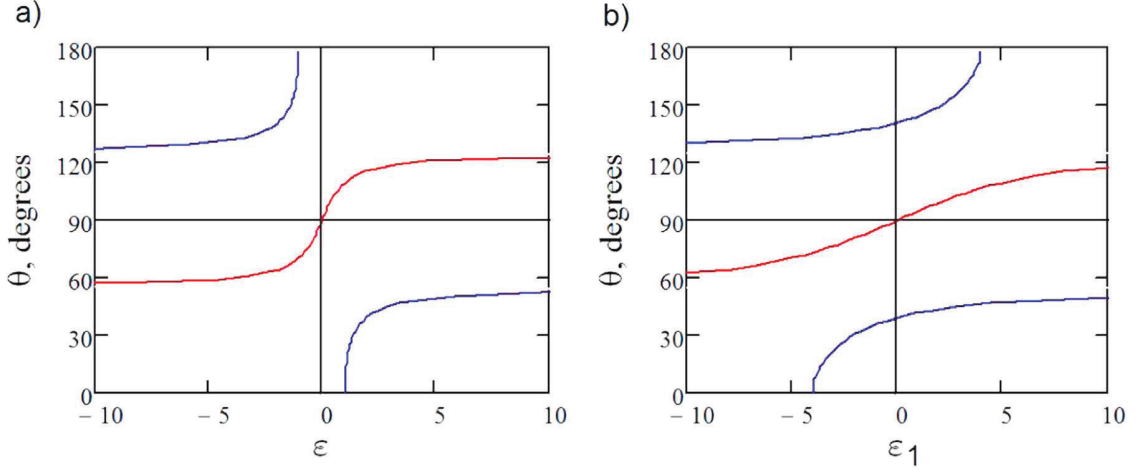


**Figure 2.** Dependence of  $\theta$  on  $\varepsilon$  and  $\varepsilon_1$  according to Equations (4) and (8), respectively. Panel (a) corresponds to the extremes of Equation (4). The red curve stands for “+” in Equation (4), and blue curves correspond to “-” in Equation (4); panel (b) shows the extremes of Equation (8). The red curve depicts the low-latitude HCS, and blue curves are additional QCSs. Note that the angles  $\theta > 90^\circ$  correspond to a QCS position in the southern hemisphere.

heliolatitudes over the entire solar cycle does not mean the absence of additional large-scale QCSs at higher heliolatitudes.

Simple calculations provided below show that the existence of a QCS at low heliolatitudes even during solar maximum is a natural consequence of the impact of the octupole component of the SMF. We will consider a superposition of (1) the dipole and octupole and (2) the quadrupole and octupole SMFs.

(1) In accordance with Equations (1) and (2), the total magnetic flux of the dipole and the octupole through a sphere around the Sun has the following view:

$$\Phi = \Phi_1 \sin^2 \theta (5 \cos^2 \theta - 1 + d), \quad (5)$$

where  $d$  is the input of the dipole to the total magnetic flux amplitude or the measure of “dipolarity.” Constant  $\Phi_1$  is defined similar to Equation (3), through the normalization on the total magnetic flux through the northern hemisphere. The magnetic flux described by Equation (5) has no more than three extrema, reflecting the location of neutral lines:

$$\begin{aligned} \theta &= \pi/2 \\ \theta &= \frac{1}{2} \arccos\left(\frac{1-d}{5}\right) \\ \theta &= \pi - \frac{1}{2} \arccos\left(\frac{1-d}{5}\right). \end{aligned} \quad (6)$$

As seen from Equation (6), neutral lines located above/below the equator appear under the condition of not very strong magnetic dipole ( $-4 < d < 6$ ) symmetrically with regard to the equatorial line. If  $d$  gradually decreases from values larger than 6 to 1, neutral lines appear at  $d = 6$  at the equator and symmetrically move away from the equator toward the poles until they reach the latitudes of  $\pm 45^\circ$  ( $\theta = 45^\circ$  and  $135^\circ$ ) at  $d = 1$ . If  $d$  changes its sign and its module increases, the neutral lines move back toward the equator until they coalesce at the equator at  $d = -4$ . As a result, the existence of either one or three neutral lines is possible (see Equation (6)).

(2) In the case of the overlapping quadrupole and octupole, the magnetic flux is

$$\Phi = \Phi_2 \sin^2 \theta (5 \cos^2 \theta - 1 + \varepsilon_1 \cos \theta), \quad (7)$$

where  $\varepsilon_1$  is a measure of the quadrupolarity in this particular case and  $\Phi_2$  is the normalization factor determined by the total magnetic flux through the northern hemisphere of the Sun. Parameters  $\varepsilon$  and  $\varepsilon_1$  reflecting a quadrupolarity are not the same, as  $\Phi_1$  and  $\Phi_2$  differ in the case of a fixed magnetic flux through the north hemisphere of the Sun. Analogous to (1), extremes of  $\theta$  from Equation (7) allocate the position of neutral lines:

$$20 \cos^3 \theta + 3 \varepsilon_1 \cos^2 \theta - 12 \cos \theta - \varepsilon_1 = 0. \quad (8)$$

Solutions of Equation (8) correspond to extremes of the magnetic flux of the overlapped quadrupole and octupole of Equation (7). These are shown in Figure 2(b). As one can see, the quadrupole magnetic field distorts the north–south symmetry. It is important to note that a symmetry violation comes from a superposition of even and odd multipole expansion terms. Similar ideas on the connection between the occurrence of the solar magnetic quadrupole and the asymmetry have been discussed in the literature (Bravo & Gonzalez-Esparza 2000).

According to Figure 2(b), the existence of either two or three neutral lines is possible in the particular case of Equation (8). At  $\varepsilon_1 = 0$ , one of the neutral lines is located near the equator (the red line in Figure 2(b)), which can be treated as the classic low-latitude HCS, while the other two are located symmetrically in the southern and northern hemispheres (the blue lines in Figure 2(b)). If  $\varepsilon_1$  increases, the HCS shifts toward the south pole, reaching  $-35^\circ$  of heliolatitudes (the polar angle  $\theta = 125^\circ$ ). Nonequatorial (blue) QCSs shift to the same direction with increasing  $\varepsilon_1$ . Then one of the QCSs disappears at the south pole at  $\varepsilon_1 = 4$  (the upper curve in Figure 2(b) reaches  $180^\circ$ ). If  $\varepsilon_1$  decreases below 0 but increases by module, the direction of motion reverses, and one of the QCS disappears at the south pole.

Therefore, three neutral lines, including the near-equatorial one, can appear under favorable conditions of the coexisting quadrupole and octupole. Since the higher harmonics of the SMF never disappear completely (Obridko et al. 2012), this may lead not only to the presence of the HCS at low heliolatitudes during all phases of the solar cycle, but also to

the coexistence of additional current sheets in the high-latitude heliosphere.

### 3. A Stationary MHD Model of QCSs

As suggested in the introduction, the SMF neutral lines may expand from the Sun to the heliosphere and become neutral sheets. If this scenario is widely applied to the HCS, the neutral lines discussed in the previous section may be described in a similar way. Consequently, the IMF may have an unexpectedly complex spatial structure, possessing several current sheets if  $\varepsilon$  or  $\varepsilon_1$  are high and the impact of the quadrupole component of the SMF is rather strong. Below we build a simple stationary MHD model, showing properties of QCSs formed in the solar wind owing to the complex multipole structure of the SMF. The model is applicable to distances of  $z \gg 1 R_\odot$  ( $R_\odot$  is the solar radius).

#### 3.1. Key Equations

We will consider the IMF vector  $\mathbf{B} = B_r \mathbf{e}_r + B_\varphi \mathbf{e}_\varphi + B_z \mathbf{e}_z$ , where  $\mathbf{e}_r$ ,  $\mathbf{e}_\varphi$ ,  $\mathbf{e}_z$  are directing vectors.  $B_r$ ,  $B_\varphi$ ,  $B_z$  are, respectively, the radial, toroidal, and vertical components of  $\mathbf{B}$ . The three components of the velocity  $\mathbf{v}$ , the current density  $\mathbf{j}$ , and the electric field  $\mathbf{E}$  can be denoted analogically. The pressure  $P$ , the plasma temperature  $T$ , and the concentration  $n$  are bounded by the equation of state:

$$P = nT. \quad (9)$$

The plasma equilibrium is described by the following equations:

$$\rho(\mathbf{v}, \nabla)\mathbf{v} = -\nabla P + \frac{1}{c}[\mathbf{j}, \mathbf{B}] \quad (10)$$

$$\text{div} \mathbf{B} = 0 \quad (11)$$

$$\text{rot} \mathbf{B} = \frac{4\pi\mathbf{j}}{c} \quad (12)$$

$$\text{rot} \mathbf{E} = 0 \rightarrow \mathbf{E} = -\nabla\phi \quad (13)$$

$$\mathbf{E} + \frac{1}{c}[\mathbf{v}, \mathbf{B}] = 0 \quad (14)$$

$$\text{div}(\rho\mathbf{v}) = 0 \quad (15)$$

$$P = K\rho^\gamma. \quad (16)$$

Here  $\rho$  is the plasma density,  $\phi$  denotes the electric potential, and  $\gamma = 1$  is the polytropic index;  $\rho = m_p n$ , where  $m_p$  is the proton mass and  $n$  is the plasma concentration. The magnetic flux  $\Phi$  and the mass flux  $F$  are defined as

$$\begin{aligned} B_r &= -\frac{\partial\Phi}{r\partial z} \\ B_z &= \frac{\partial\Phi}{r\partial r} \\ \rho v_r &= -\frac{\partial F}{r\partial z} \\ \rho v_z &= \frac{\partial F}{r\partial r}. \end{aligned} \quad (17)$$

The main suppositions of the model are listed below.

1. It is possible to perform a substitution of variables, having a transition from  $(r, z)$  to  $(r, \Phi)$  in the areas between extremes of the magnetic flux. Since  $\Phi = \text{const}$

at the neutral sheets, magnetic field lines cannot cross current sheets, and magnetic loops are not formed, which is in agreement with the open flux paradigm (Pneuman & Kopp 1971).

2. The solar wind is super-Alfvénic and suprathermal:  $v_r \gg v_A$ ,  $v_T$ . This supposition suggests that one can neglect the terms proportional to the Alfvénic speed  $v_A$  and the thermal speed  $v_T$  if it is necessary to calculate their sum, for example, in Equation (10).
3.  $\frac{\partial}{\partial r} \left( \frac{\partial\Phi}{r\partial r} \right) \ll \frac{\partial^2\Phi}{r\partial z^2}$  in Euler's equation with the Ampère's force of Equation (10). In other words, spatial variations of the magnetic flux along  $z$  change faster than variations along  $r$ .

Taking into account the suppositions listed above, one can integrate Equations (10) and (14) over  $r$ . Details of the calculation can be found in the appendix of Kislov et al. (2015). The resulting algebraic expressions of Equations (18)–(23) represent solutions of Equations (9)–(16):

$$v_r^2 = 2U(\Phi) \quad (18)$$

$$\rho v_p = \alpha(\Phi) B_p \quad (19)$$

$$v_\varphi = \frac{\alpha\Psi(\Phi) - \rho\Omega r^2}{4\pi\alpha^2 r} \quad (20)$$

$$\Omega = c \frac{\partial\phi(\Phi)}{\partial\Phi} \quad (21)$$

$$B_\varphi = \rho \frac{\Psi(\Phi) - 4\pi\alpha\Omega r^2}{4\pi\alpha^2 r} \quad (22)$$

$$\rho = \frac{2\pi v_T^2 \alpha^2}{2U + \Omega^2 r^2} \left( -1 + \sqrt{1 + \rho_0(r) \frac{2U + \Omega^2 r^2}{\pi v_T^2 \alpha^2}} \right). \quad (23)$$

$U$ ,  $\alpha$ ,  $\Omega$ , and  $\Psi$  are functions of the magnetic flux  $\Phi$ . They are supposed to be known near the Sun. The flux functions can be traced along magnetic field lines from the area where they are initially determined to the area of modeling. The  $\alpha$  parameter has the meaning of the mass download of magnetic field lines, and its form depends on the latitudinal distribution of the mass flux density on the Sun. Also,  $\alpha = dF/d\Phi$ . One can find that an unambiguous dependence between the two magnetic fluxes comes from Equations (11), (15), and (19) (Kislov et al. 2015). Function  $U$  determines the main component of the solar wind speed. The variable  $\Omega$  is the Ferraro isorotation angular speed. It is responsible for a partial corotation of the solar wind with the Sun along magnetic field lines. Flux function  $\Psi$  manages the angular momentum transfer, and  $\rho_0(r)$  is the plasma density at the equator ( $z = 0$ ).

Equation (10) is reduced to the quadrature with Equations (17)–(23). As a result of the numerical integration, a function  $z(r, \Phi)$  can be found, which is an implicit expression that allows us to determine both  $\Phi(r, z)$  and the magnetic flux functions as functions of coordinates. As follows from Equations (17) and (19),

$$z(r, \theta) = \frac{1}{r} \int_\theta^{\pi/2} \frac{\alpha(\Phi(\sigma))}{\rho(r, \Phi(\sigma)) v_r(\Phi(\sigma))} \frac{\partial\Phi(\sigma)}{\partial\sigma} d\sigma, \quad (24)$$

where  $\Phi(\sigma)$  is the magnetic flux in a form of Equations (3), (5), or (8). It is assumed that  $\Phi = 0$  at the north pole of the Sun. Equation (24) can be solved numerically. Using Equations (3),

(5), or (8), the dependency  $z(r, \theta)$  can be represented as  $z(r, \Phi)$ , where  $\Phi$  is monotonic over  $\theta$ .

Therefore, the problem can be reduced to choosing magnetic flux functions  $U$ ,  $\alpha$ ,  $\Omega$ , and  $\Psi$ . A transition from flux variables to spatial variables can be performed by the integration of Equation (24). The model has five parameters:  $\rho_{\text{sph}}$  is the plasma density on the boundary sphere,  $v_T$  is the thermal speed,  $m$  is the total mass flux from the Sun,  $M$  denotes the ratio of  $m$  to  $\Phi_0$  (i.e., the amplitude of  $\alpha$ ), and  $\varepsilon$ ,  $\varepsilon_1$ , or  $d$  characterizes the impact of the quadrupole or dipole depending on a specific case (see above).

### 3.2. Selection of Flux Functions

We will describe below the suppositions that allow us to determine a form of the flux functions  $U(\Phi)$ ,  $\alpha(\Phi)$ ,  $\Omega(\Phi)$ ,  $\phi(\Phi)$ , and  $\Psi(\Phi)$ . Their values have been selected in accordance with Kislov et al. (2015). Let us consider a sphere around the Sun with the radius of  $R_0 = 20 R_\odot$ , where  $R_\odot$  is the solar radius. By assumption, latitudinal distributions of plasma parameters at the sphere are the same as in the solar corona. The position of the boundary sphere is chosen far enough from the Sun to never cross the Alfvénic surface.

The main expression for the magnetic flux is Equation (3). We will also employ Equations (5) and (7) for the cases when the octupole component of the SMF is taken into account.

We assume that the mass flux density does not depend on latitude. Then

$$\rho v_r^2 = \text{const}|_{r=20R_\odot}. \quad (25)$$

This is the simplest representation of the uniform plasma outflow to all latitudinal directions. Parker's model is based on the same assumption (Parker 1958). Therefore, the angular dependence of the mass flux on the boundary sphere can be found as

$$F(\theta) = 0.5m(1 - \cos \theta). \quad (26)$$

Here  $m = 7 \times 10^{11} \text{ g s}^{-1}$  is the total mass flux of the Sun. The mass download of the magnetic field lines  $\alpha$  can be determined with help of Equation (3) as a derivative of Equation (26) with respect to the magnetic flux  $\Phi$ :

$$\alpha = \frac{\partial F / \partial \theta}{\partial \Phi / \partial \theta}.$$

The unipolar induction in the solar photosphere determines the magnitude of the electric potential. For a simplification of the model, electric currents between the corona and the photosphere are not taken into account here, although related possible effects may also exist, as shown in Kislov et al. (2015). As follows from Parker (1958), the solution in Equation (20), and the absence of  $B_\varphi$  near the Sun,  $d\phi = \frac{\omega(\Phi)d\Phi}{c}$ . Here,  $\omega(\Phi)$  is the angular speed of plasma rotation in the photosphere. Hence, we can find the flux function:

$$\Omega = \omega(\Phi), \quad (27)$$

where  $\omega(\theta) = \omega_p(1 + 0.7(\sin^2 \theta + \sin^4 \theta))$  can be written as  $\omega(\Phi)$  with the help of Equations (3), (5), or (7) (adapted from Snodgrass 1983) and  $2.4\omega_p$  is the angular velocity of the rotating photospheric plasma at the solar equator.

Note that although the model cannot be applied to the photosphere, the “frozen-in” condition in Equation (14) and its consequence in Equations (20) and (22) are correct there. The reason is that the assumption of thin current sheets is not used in deriving of Equations (20) and (22), and  $\Omega$  can be translated to the region of calculations not only from a chosen sphere around the Sun but directly from the photosphere. The form of  $\omega$  is the same as in Kislov et al. (2015), that is, it represents the sum of even degrees of sines of  $\theta$ . The expressions in Equations (20) and (22) are also used to set the azimuthal magnetic field on the sphere.

Let us consider the plasma density  $\rho_0(r)$  along the main neutral line. It is defined as

$$\rho_0(r) = \frac{\rho_{\text{sph}} R_0^2}{r^2} \quad (28)$$

in accordance with a well-known reverse-squared radial dependence of the plasma density on distance in the heliosphere. Finally, the concentration at the sphere of  $R_0 = 20 R_\odot$  according to Maiewski et al. (2018) is

$$n_1 = 500(1 - 0.34 \cos^2 \theta) \text{ cm}^{-3}. \quad (29)$$

Therefore,  $\rho_{\text{sph}} = 500 m_p (\text{g cm}^{-3})$ , where  $m_p$  is the proton mass.

As a result, the radial component of the velocity at  $20 R_\odot$  is

$$v_r = \frac{m}{4\pi m_p n_1 R_0^2}. \quad (30)$$

We can obtain all unknown functions in (Equations (18)–(23), which allows us to find  $\Phi(r, z)$ , using Equation (24)). To do so, it is necessary to substitute all obtained functions of Equations (25)–(30) for (18)–(23), taking Equations (3), (5), or (7) into account.

## 4. Results

### 4.1. Solutions with the Quadrupole Component of the SMF

Figures 3–6 illustrate the behavior of plasma and IMF parameters in the solar wind based on the solutions of the model at the Earth's orbit. Figure 3 is organized in the way of two vertical panels representing the “parameter versus distance along  $z$  at 1 AU” solutions for the case (1) of a pure dipole (the left panel) and (2) the coexistent dipole and quadrupole SMFs (the right panel). Therefore, Figure 3(a) shows the radial component of the IMF for the pure dipole magnetic field, and Figure 3(b) illustrates the behavior of the same parameter for the dipole-quadrupole case. An analogous scheme is applied to the plasma density (c), (d), the azimuthal IMF component (e), (f), and the radial component of the velocity (g), (h).

In the pure dipole case, the parameters have a classic symmetric view with an extremum at  $z = 0$ . Meantime, two nonsymmetric neutral surfaces appear in all panels in the case of the significant quadrupolarity  $\varepsilon$ . Furthermore, as seen in Figure 3(b), none of the two  $B_r$  surfaces has an equatorial position, although one of the surfaces is located closer to the equatorial plane and may be treated as the displaced HCS. The density peaks in Figures 3(c) and (d) correspond to QSC positions revealed from the  $B_r$  behavior.

In the case of the overlapping dipole and quadrupole (Figure 3(d)), the density grows abruptly at current sheets determined by the position of the  $B_r$  peaks shown in

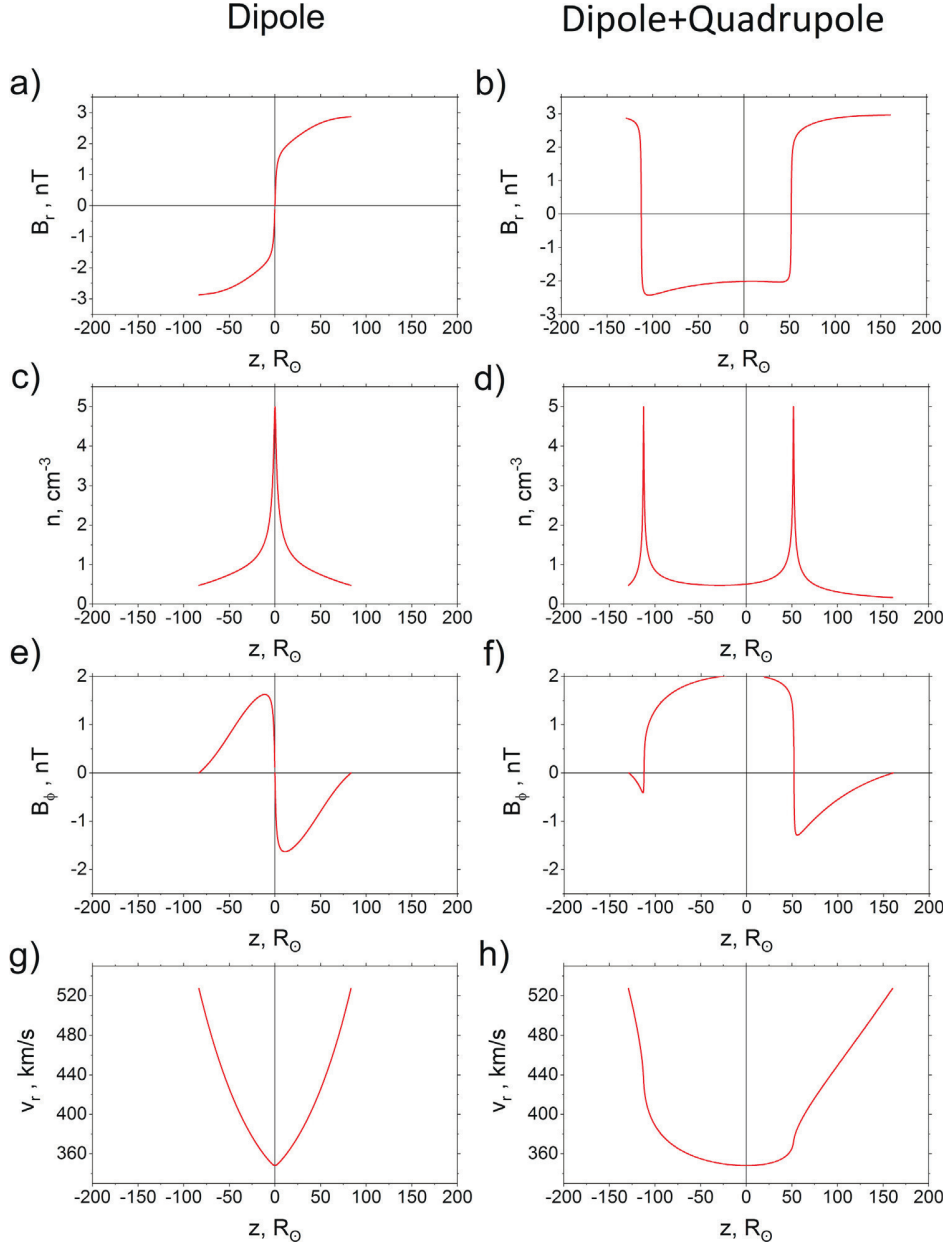


**Figure 3.** 1 au meridional profiles of the radial IMF component (a), (b), the plasma concentration (c), (d), the azimuthal IMF component (e), (f), and the radial component of the velocity (g), (h) in the cases of the pure dipole (the upper panel) and the overlapping dipole and quadrupole magnetic fields of the Sun, at  $\varepsilon = 2$ .

Figure 3(b). The existence of two neutral lines in the right panel is also obvious from the behavior of the azimuthal IMF component (compare Figures 3(e) and (f)). This is a result of the  $B_\phi$  dependency on  $B_r$ , which originates from the heliospheric plasma rotation and the unipolar generation of  $B_\phi$  (see Equations (20) and (22) and Kislov et al. 2015).

The solar wind speed shown in Figures 3(g) and (h) is calculated as a projection of the latitudinal distribution of the speed near the Sun to a certain point in the solar wind. The obtained solution reflects the fact that the solar wind is fast at high latitudes and slow at low latitudes in solar minimum (Figure 3(g)). In the case of the mixed dipole and quadrupole (Figure 3(h)), the solar wind speed is asymmetric with respect to the equator, similar to the other parameters. Applying Equation (18) and knowing the magnetic flux in the area of

interest, it is possible to find an analytic solution for the solar wind speed, using observed profiles of the speed near the Sun as shown by Khabarova et al. (2018).

The azimuthal component (Figures 4(a), (b)) and the radial component of the current density (Figures 4(c), (d)) demonstrate similar tendencies noticed in Figure 3. The left panel of Figure 4 is for the pure dipole case, and the right panel is for the dipole-quadrupole combination. The density of currents flowing along two current sheets in the complex case of coexistent dipole and quadrupole magnetic fields has the opposite direction in two hemispheres (Figures 4(b) and (d)). As a result, the two currents have a tendency to repel according to Ampere's force law. This means that such current sheets tend to repulsion and cannot merge further from the Sun even if they are disturbed and pushed to each other by high-speed



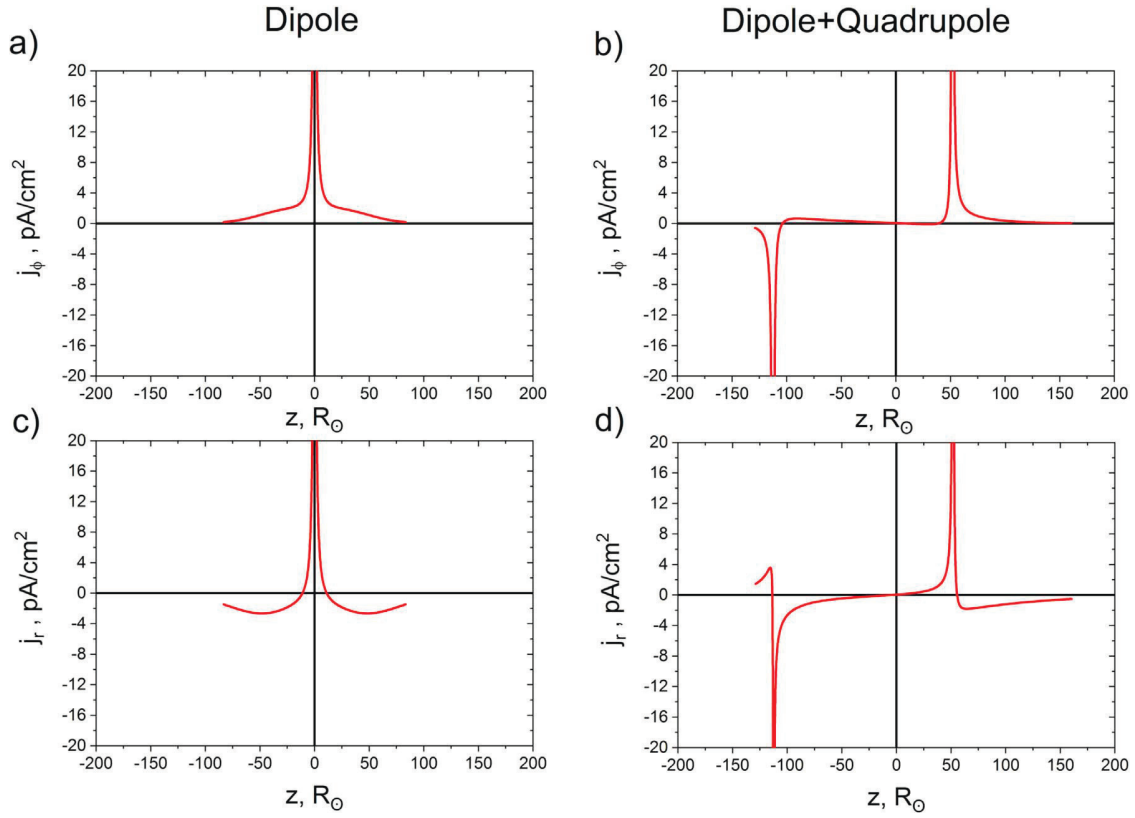


**Figure 4.** 1 au meridional profiles of the azimuthal component of the current density (a), (b) and the radial component of the current density (c), (d) under the condition of the pure dipole SMF (the left panel) and the overlapping dipole and quadrupole magnetic fields, at  $\varepsilon = 2$  (the right panel).

streams, which often occurs in the solar wind (see Khabarova et al. 2016). Consequently, one may expect to observe two large-scale current sheets at different heliolatitudes rather far from each other.

We should note that the azimuthal current density can reach overestimated values in the nearest vicinity of the neutral surface. This is a consequence of the nonapplicability of the MHD model to the investigation of fine structure of thin current sheets because the mass download parameter  $\alpha$  tends to infinity near neutral surfaces and its sign reverses at the crossing of these surfaces.

The other important point is that the north–south symmetry gets broken at any nonzero  $\varepsilon$ , as illustrated in Figure 5. Figure 5(a) shows the position of neutral surfaces in the  $(z, r)$  plane in the inner heliosphere. The two current sheets labeled “1” occur at  $\varepsilon = 2$ , corresponding to the strong quadrupole magnetic field case, and at  $\varepsilon = 0.9$ , when the quadrupole magnetic field is relatively weak, only one current sheet exists that may be treated as the classic HCS. The shape of neutral surfaces is not radial closer to Sun, at heliocentric distances less than 0.5 au for both values of  $\varepsilon$ . At the same time, the lines in Figure 5(a) are almost straight in the meridional cross-section at large distances; therefore the corresponding 3D neutral surfaces tend to be conic with distance. This is in agreement with results of the models based on the source surface hypothesis obtained for quite different boundary conditions (Owens & Lockwood 2012; Wang 2014). The position of the neutral surface 2 in Figure 5(a) is closer to the equatorial plane than that of curves 1, which is a consequence of the fact that the larger  $\varepsilon$  corresponds to the stronger magnetic field and vice versa, so under the condition of a weak quadrupole component, one can

expect to find the only current sheet near the equator. If a sign of the quadrupolarity  $\varepsilon$  changes, then the displacement of current sheets has the opposite direction, that is, all plots become mirrored with respect to the equator.

Figure 5(b) shows the radial dependence of  $B_r$  in the inner heliosphere according to the model (curve I). As seen in Figure 5(b), the estimated equatorial magnetic field at the Earth’s orbit is about 1.8 nT, which is in a good agreement with in situ observations.

In agreement with Parker’s model (Parker 1958) and its generalizations (i.e., Weber & Davis 1967), the radial IMF component decreases with heliocentric distance with a slope of  $-2$ . It has been shown that the observed dependence is closer to  $-5/3 = -1.66$  (Khabarova & Obridko 2012; Khabarova 2013). In our model,  $B_r$  decreases as  $r^{-1.35}$ , that is, the slope is close to  $-4/3$ . The approximation of the solution at the equator has a view of  $B_r = 41.91(20R_\odot/r)^{1.36}$  nT (see Figure 5(b), curve II), which is likely a result of the azimuthal asymmetry of the QCS. This finding supports a suggestion by Khabarova & Obridko (2012) that the occurrence of the HCS impacts spatial characteristics of the IMF at low heliolatitudes and causes the discrepancies between the observed and predicted slope of the  $B_r(r)$ .

We have obtained solutions that describe profiles of the plasma and IMF and characterize the position and properties of QCSs in the solar wind. The IMF, the density, and the current density sharp changes clearly denote the location of current sheets formed in the solar wind at different conditions at the Sun, which are determined by a combination of the dipole SMF and its higher harmonics. In this section, we considered the following conditions: (1) the pure dipole magnetic field of the

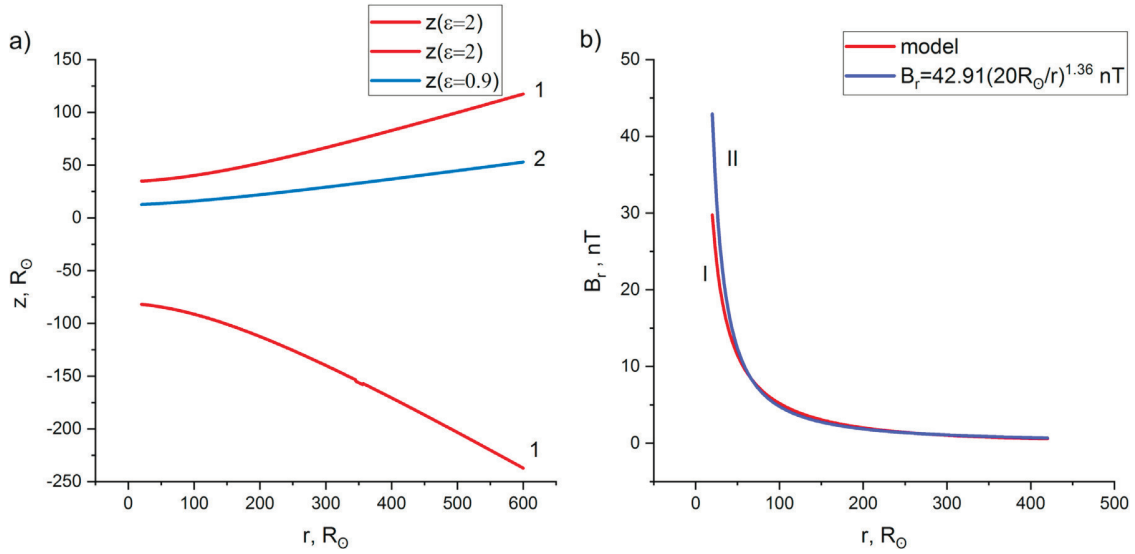


**Figure 5.** Location of the neutral sheets (a) and the radial dependence of  $B_r$  (b). (a) Example of the location of neutral sheets in the inner heliosphere under the condition of the overlapping dipole and quadrupole. The meridional cut. Numbers 1 and 2 in the panel correspond to different inputs of the quadrupole component of the SMF. Curves 1:  $\varepsilon = 2$  (the strong quadrupole case). Curve 2:  $\varepsilon = 0.9$  (the weak quadrupole). (b) Dependence of the radial IMF component on heliocentric distance at  $z = 0$  and  $\varepsilon = 2$ . According to the model (line I),  $B_r$  at 1 au is  $\sim 1.8$  nT. Line II is the approximation of solution I at the equator with  $B_r = 41.91(20R_\odot/r)^{1.36}$  nT.

Sun and (2) the superposition of the dipole and the quadrupole SMFs. Summarizing, (1) more than one QCS may exist in the heliosphere, and (2) the position of a QCS in the solar wind significantly differs from a simple projection of the initial neutral line at the Sun.

#### 4.2. The Impact of the Octupole Component of the SMF on the Number and Position of Current Sheets in the Solar Wind

In addition to the study of a possible impact of the quadrupole on the picture of current sheets in the inner heliosphere, we will consider below the problem of the nonzero octupole component of the SMF. The solutions are built for the magnetic flux calculated according to Equation (5) with  $d = -2$ , which corresponds to the overlapping dipole and octupole, and with  $\varepsilon_1 = -2$ , which corresponds to overlapping quadrupole and octupole. In the left panel of Figure 6 are found the solutions for the “dipole-octupole” case, and the right panel shows the solutions for the same parameters in the “quadrupole-octupole” case. In the case of mixed quadrupole and dipole magnetic fields, there are either two or three current sheets (as seen in the left panel of Figure 6). The main peculiarity of the solution with a strong octupole is the existence of a current sheet near the equator. This makes the picture very realistic because it corresponds to observations of the HCS near the ecliptic plane even at solar maximum. This can be seen in Figures 6(a), (e), (j). Thus, Figure 6(a) shows the position of two neutral surfaces located symmetrically with respect to the equator and one current sheet located directly at the equator. Figure 6(b) shows the tangent tilt angle to a neutral surface in the corresponding case. It is easy to find that the angle gradually comes to a constant, which means a “straightening” of neutral surfaces with distance. As a result, at far distances from the Sun, 3D neutral surfaces have the shape of cones, and the corresponding straight lines in the meridional cut are nonradial, as seen in Figures 6(a), (b). Since the existence of neutral surfaces determines the global structure of the heliospheric magnetic field, the latter should

consequently be nonradial as well. This can be taken into account at the building of global models of the heliosphere. The corresponding deviations from radially nevertheless can be small near the ecliptic plane where most observations take place.

The pattern of the curves in the left panel of Figure 6 is symmetric as the chosen tensor of the octupole moment is diagonal in the system of coordinates that is used here. Meanwhile, in the case of the superposed octupole and quadrupole magnetic fields, the north–south asymmetry becomes significant, which again may give an additional clue to explain the observations of the well-known HCS displacements (see Mursula & Hiltula 2003 and references therein).

Figure 6(b) shows the position of neutral surfaces for the quadrupole-octupole combination of the SMF. The magnetic flux is set in accordance with Equation (7) at  $\varepsilon_1 = -2$ . The violation of symmetry takes place for all neutral lines owing to the shift of all QCSs to the same pole at nonzero  $\varepsilon_1$ . As a result, initial neutral lines located symmetrically expand with distance in the form of surfaces that position changes asymmetrically. In the case shown in Figure 6(b), the corresponding current sheets have a conic form at far distances, analogous to the previous case (Figure 6(a)).

Figures 6(e)–(h) are plotted to prove that the neutral surfaces identified by the extrema in Figures 6(a), (b) indeed correspond to flows of the current in both the dipole-octupole and the quadrupole-octupole case. Figures 6(e) and (f) show the azimuthal projections of the current density. Figures 6(g) and (h) represent the radial projections of the current density. In the right panel, again, the presence of the quadrupole results not only in asymmetry of currents sheets with regard to the equator but also in their regular shift with distance from the initial position of the “mothering” neutral line at the Sun. This fact shows the importance of studying the spatial evolution of current sheets in the heliosphere.

As an example of a possible situation that may occur in the solar wind when the solar dipole weakens, we show a 3D

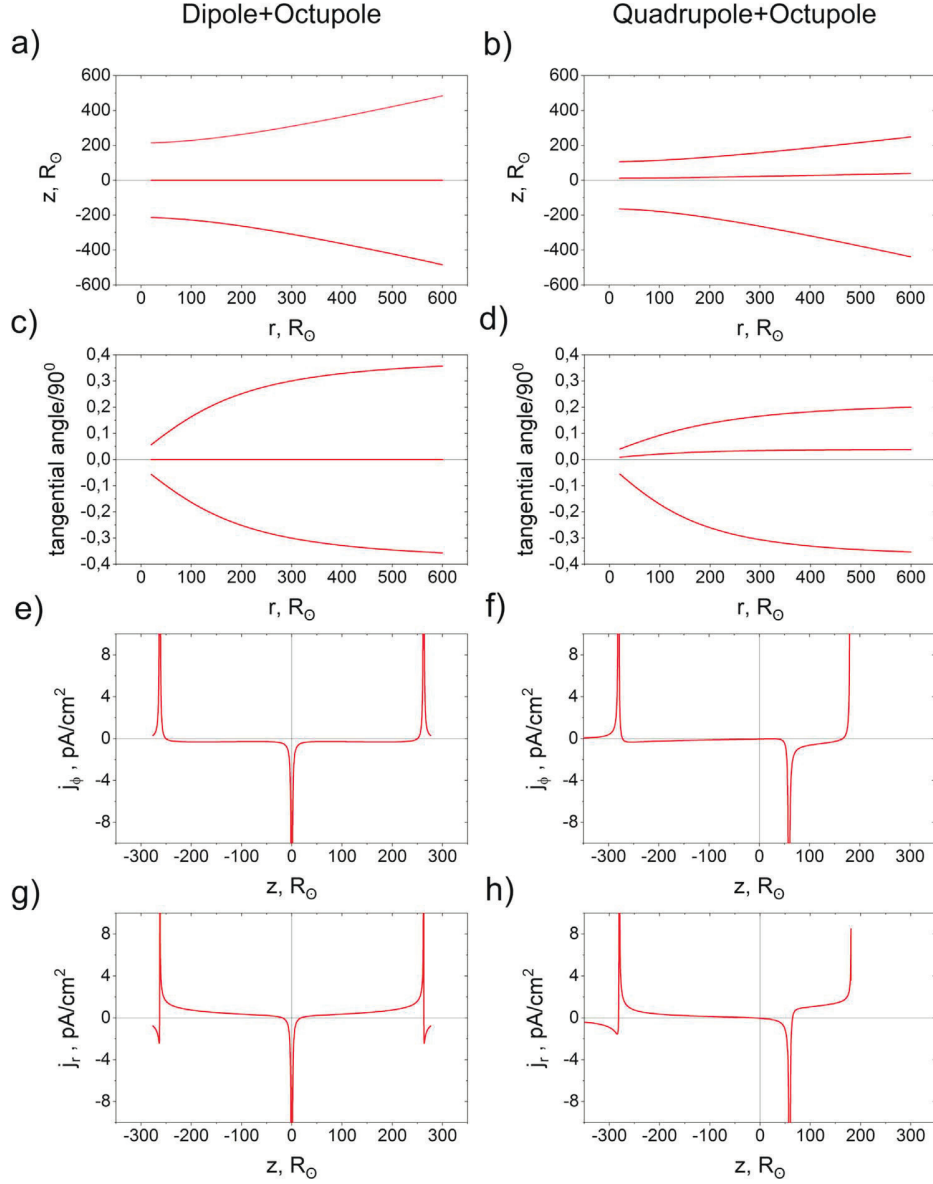


**Figure 6.** Key parameters of neutral sheets in the solar wind. Left panel stands for the dipole-octupole case at  $d = -2$ . Right panel shows solutions for the quadrupole-octupole case at  $\varepsilon_1 = -2$ . (a), (b) Meridional cut of the neutral surfaces; (c), (d) tangential angle to the neutral surface (normalized to  $90^\circ$ ); (e), (f) and (g), (h) are the azimuthal and radial components of the current density, respectively. Meridional cut, the Earth's orbit.

version of the modeling obtained for the simple, symmetric octupole-dipole case corresponding to the left panel of Figure 6. In Figure 7, the two higher-latitude current sheets possess a conic shape, and one current sheet, corresponding to the HCS, is located at the magnetic equator. In reality, current sheets are always disturbed owing to both various instabilities along their surface and the propagation of high-speed streams. In the simplest case, current sheets possess a wavy form, which allows in-ecliptic spacecraft to reveal a sector structure of the IMF while crossing the wavy HCS. Khabarova et al. (2015, 2016, 2017b) have shown that the real HCS is far more waved (or rippled) than suggested by many models showing the existence of the merely slightly wrapped HCS. For illustrative purposes, we subsequently multiplied the solution given in Figure 6(a) to  $\sin 4\varphi$  and to  $\sin 8\varphi$  to imitate a real situation in the quiet solar (here,  $\varphi$  is the azimuthal angle). One

can see the corresponding modified form of the three current sheets in Figures 7(b) and (c).

It is obvious that in the periods far from the solar minimum a spacecraft located near the ecliptic plane crosses the current sheet (the green surface) many times as the solar wind rotates. As noted above, the current sheet nearest to the ecliptic plane can be treated as the HCS. At the same time, a spacecraft located above the ecliptic plane may also repeatedly cross an SCS, which is not the HCS but one of additional strong QSCs formed in the heliosphere (the red and blue surfaces in Figures 7(b) and (c)). In reality, situations occurring in the solar wind are always more complex than predicted by any quasi-stationary model; therefore one may expect to observe current sheets not only intensively waved but also disrupted by fast solar wind streams.

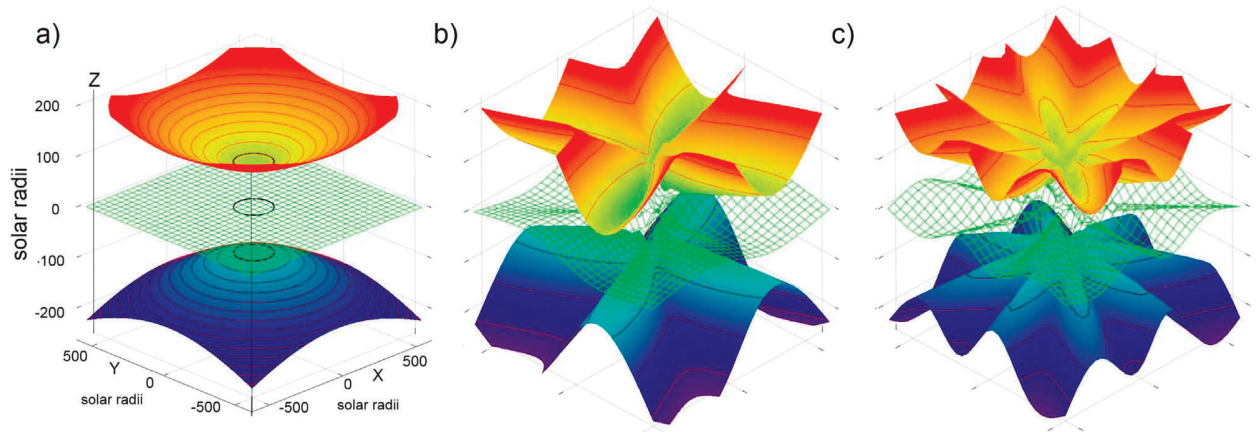


**Figure 7.** 3D current sheets that occur in the heliosphere under the condition of the superposed solar dipole and octupole magnetic fields at  $d = -2$ . The green current sheet may be treated as the HCS. (a) No disturbances. Panels (b) and (c) show the disturbed current sheets.

## 5. Discussion and Conclusions

Solar observations show that although the situation at the Sun is changeable, there are long-lived stable regions with the magnetic field of the opposite polarity (Ness & Wilcox 1964; Edmondson et al. 2010). There is a tendency in the literature to admit the occurrence of numerous magnetic separators and neutral lines at the Sun (Edmondson et al. 2010; Titov et al. 2012), but talking of the solar wind, the existence of only one current sheet, namely, the HCS located near the solar equator, is usually admitted (e.g., Mikić et al. 1999). In the meantime, most stable magnetic separators at the Sun should correspond to QCSs, otherwise the plasma balance is not fulfilled and a system of several magnetically independent regions stops existing very quickly. As noted above, one may expect that all quasi-stable neutral lines observed at the Sun (or at the source surface) extend to the heliosphere as current sheets, and obviously only one of them can be treated as the HCS observed at the Earth’s orbit.

A goal of this study was to show a high probability of the occurrence of multiple current sheets in the heliosphere under the condition of coexistence of the dipole and quadrupole/octupole magnetic fields of the Sun at any phase of the solar cycle apart from the deep solar minimum. We have built a model that can be attributed to the class of so-called “cylindrical wind” models, since they employ cylindrical solutions. Such models are common in astrophysics and often applied to the description of stellar winds (Heyvaerts & Norman 1989; Vlahakis et al. 2000; Drake et al. 2015). A frequent argument in favor of using a spherical geometry in the solar wind and heliospheric models is that the magnetic field of the Sun and, consequently, of the solar wind is supposed to be spherically symmetric (Parker 1958). Meanwhile, it contradicts the observations of the solar corona (Pneuman & Kopp 1971; Bemporad 2017) and is not entirely accurate in the heliosphere (Smith 2001; Khabarova & Obridko 2012; Khabarova 2013; Khabarova et al. 2018). In order to obtain semianalytical solutions depending on latitude, we have employed the axial symmetry as a reasonable and convenient technical feature to build our model. General characteristic properties of cylindrical winds are (1) an axial symmetry, (2) a cylindrical- or disk-shaped plasma source, and (3) the corresponding form of magnetic field lines. At large distances from the axis of cylindrical symmetry, the behavior of parameters is often

similar to that obtained by models with a spherical source surface. It should be noted that an axisymmetric model (Kislov et al. 2015) used as a basis of the current sheet model is inapplicable near the Sun.

A stationary one-fluid axisymmetric ideal MHD model built in this study predicts the location, form, and number of current sheets in the solar wind determined by the input of quadrupole and octupole components in the global magnetic field of the Sun. The main results can be formulated as following.

1. In the case of a pure dipole, only one current sheet exists in the solar wind, representing an extension of the magnetic equator. This case obviously corresponds to the classic picture of the low-latitude HCS in solar minimum.
2. In the case of the overlapping dipole and quadrupole SMFs, either one or two current sheets of a conical form may exist in the solar wind.
3. The strong octupole SMF overlapped with the dipole leads to the formation of three current sheets in the heliosphere. One is located at the equator, and the other current sheets form two cones that are symmetric with respect to the equator. The conic current sheets may disappear if the dipole component dominates.
4. The superposed octupole and quadrupole magnetic fields of the Sun also produce three current sheets, but in this case the current sheets may be asymmetric with respect to the equator.
5. The north–south asymmetry of the IMF is a natural consequence of the impact of the quadrupole harmonic of the SMF on the picture of the magnetic field in the heliosphere. This conclusion is in good agreement with prior works, for example, Bravo & Gonzalez-Esparza (2000).
6. The radial IMF component decreases with distance not following the  $r^{-2}$  law near the helioequator. The model returns the slope of  $-4/3$ , which is rather close to that observed in the inner heliosphere (Khabarova & Obridko 2012; Khabarova 2013). This suggests that both the north–south asymmetry of the IMF resulting from the presence of the quadrupole SMF and the occurrence of an SCS at low heliolatitudes impact the dependence of  $B_r$  on heliocentric distance. As a result, the observed  $B_r(r)$  slope of  $-5/3$  differs from the  $-2$  slope predicted by Parker-like models. This confirms the idea of Khabarova &



Obridko (2012) about a possible impact of the HCS on the radial evolution of  $B_r$  at low heliolatitudes.

A significant role of the quadrupole component of the magnetic field of the Sun in the emergence of the north–south asymmetry in the heliosphere was studied in detail (Osherovich et al. 1984, 1999; Bravo & Gonzalez-Esparza 2000). It was shown that in the period of a polarity reversal, the quadrupole (but not octupole) harmonic of the SMF prevails, being one order larger than dipolar. Recent modeling by Usmanov & Goldstein (2013) shows that an insignificant asymmetry occurring at the Sun practically disappears by 16 solar radii, which cannot explain observations of the phenomenon observed much further from the Sun (e.g., Bravo & Gonzalez-Esparza 2000). In our model, the asymmetry is visible through the heliosphere. At the Earth’s orbit, it appears with an opposite sign because of the difference of the magnetic pressure between the two hemispheres of the heliosphere. It is worth noticing here that because of the centrifugal force, magnetic field lines tend to be extended along the equator (i.e., along the normal to the solar rotation axis). Therefore, the effects of the asymmetry can decrease with distance at low heliolatitudes but be apparent at higher heliolatitudes, as shown in a recent observational study (Khabarova et al. 2018).

The heliosphere with the pure quadrupole or the octupole magnetic field of the Sun was modeled by Reville et al. (2015). However, the impact of superposed dipole–quadrupole, dipole–octupole, or quadrupole–octupole SMFs on the structure of the heliosphere was not considered there, since the work was aimed at the estimation of losses of the moment of impulse of stars with various magnetic fields. Osherovich et al. (1999) and Usmanov & Goldstein (2013) have not considered the quadrupole SMF strong enough to impact the entire heliosphere either.

It is always difficult to compare different models, but we would like to note that despite the differences indicated above there are similarities with some of the prior models. Schultz (1973, 2007, 2008) has built models with a nonspherical source surface, taking into account the quadrupole SMF and consequently obtaining solutions with conic current sheets. The model (Schultz 1973) is non-self-consistent, contrary to ours, but the possible existence of stable QCSs in the heliosphere is claimed similarly. Banaszkiewicz et al. (1998) have built a “dipole plus current sheet” non-self-consistent model, not considering the plasma density but taking into account differential rotation of the Sun analogous to our approach, which has led to realistic conclusions on the IMF spiral characteristics and the north–south asymmetry. Generally, our model is rather far from Parker-like models (e.g., Pizzo 1982) in which the total velocity and the IMF are parallel to each other in a noninertial reference system, but it is in a good agreement with Banaszkiewicz et al. (1998), Bravo & Gonzalez-Esparza (2000), and empirical models like those suggested by Smith & Bieber (1991). Therefore, our model may be treated as a supplement to prior models. In this study we emphasize the fact that the global picture of current sheets in the heliosphere may be more complex than suggested before.

The results obtained in the study may be useful for building global models of the heliosphere. It should be noted that the existence of more than one QCS in the heliosphere offers wide possibilities for the development of models of the transport of cosmic-rays and energetic particles in the heliosphere. Cosmic rays and energetic particles are known to propagate most easily

along magnetic field lines and especially along the HCS. Numerous studies show the importance of the form and strength of a current sheet for the particle transport (see Sternal et al. 2011; Burger 2012; Pizzella 2018; Engelbrecht 2019 and references therein). Furthermore, modeling shows that the HCS is found to impact the propagation of solar energetic particles (Battarbee et al. 2017), which may also be applied to other SCSs. If there are more quasi-stable ways for galactic or Jovian cosmic rays to propagate to the inner heliosphere and for solar cosmic rays to the outer heliosphere, this may explain the observed unusual features of the energetic particle flux better. Certainly, there should be interesting kinetic-level effects related to turbulent areas surrounding QCSs that may impact the propagation of energetic particles along QCSs, but this issue cannot be resolved in the frames of our simple MHD model and should be considered separately. One may just speculate that in solar maximum, when the HCS is strongly disturbed by low-latitude high-speed streams and flows coming from both active regions and coronal holes, high- and middle-latitude QCSs in turn may become the main undisturbed channels of energetic particles in the global heliosphere.

One more application of the model lies in the astrophysical sphere. According to modern theories of the stellar dynamo (e.g., Moss et al. 2008), there should be stars with the complete absence of the dipole component of the stellar magnetic field. If so, more than one stable current sheet should definitely exist in their astrospheres, which potentially may be useful for understanding the dynamics of stellar winds.




From the observational point of view, it should be taken into account that it is not quite correct to associate the position (or the latitude) of a neutral line on the Sun with the position/latitude of the corresponding current sheet in the heliosphere. First of all, the solar rotation and other dynamical effects may lead to a significant change of the shape of a particular current sheet. This, together with the impact of fast streams/flows, may be one source of disagreement between theoretical expectations for finding the HCS in a particular place and observations. An analysis of the HCS crossings in the heliosphere poorly corresponds to predictions if one assumes the HCS to be a simple radial projection of the solar magnetic equator (Suess et al. 1995). The disagreement may be a signature of distortion of the current sheet in the solar wind by different streams and instabilities but also may result from the MHD-determined change of its form as it does not obey a simple radial expansion of the solar wind.

In this study, we show that another source of a potentially incorrect interpretation of observations of current sheet crossings may arise from the initial underestimation of the number of QCSs in the solar wind. In other words, if solar observations show the occurrence of a magnetic separator at the Sun at relatively high heliolatitudes, solar wind observations may show the current sheet crossing far from the same heliolatitudes. Furthermore, not every crossing of an SCS in the solar wind may correspond to the HCS crossing. It may be one of the additional disrupted QCSs detected by a spacecraft instead. This suggests a serious reconsideration of observations from the *Ulysses* spacecraft and other spacecraft that measured the solar wind far from the ecliptic plane.

The authors are grateful to V.N. Obridko, E.V. Maiewski, D. D. Sokoloff, A. Usmanov, and A.A. Korolev for useful discussions. We also thank the unnamed referee for inspiring

questions and suggestions. This work is partly supported by the International Space Science Institute (ISSI) in the framework of International Team 405 entitled “Current Sheets, Turbulence, Structures and Particle Acceleration in the Heliosphere.” R.A. K. and H.V.M.’s work is partially supported by RFBR grants 17-02-01328 and 19-02-00957. O.V.K. acknowledges RFBR grants 17-02-00300, 17-02-01328, 18-52-06002, and 19-02-00957.

## ORCID iDs

Roman A. Kislov  <https://orcid.org/0000-0002-5609-7572>  
 Olga V. Khabarova  <https://orcid.org/0000-0002-3230-2033>  
 Helmi V. Malova  <https://orcid.org/0000-0001-6511-2335>

## References

- Alfvén, H. 1977, *RvGSP*, **15**, 271  
 Alfvén, H. 1981, *Cosmic Plasma*, Astrophysics and Space Science Library, Vol. 82 (The Netherlands: Springer)  
 Antonucci, E., & Svalgaard, L. 1974, *SoPh*, **36**, 115  
 Banaszkiewicz, M., Axford, W. I., & McKenzie, J. F. 1998, *A&A*, **337**, 940  
 Battarbee, M., Dalla, S., & Marsh, M. S. 2017, *ApJ*, **836**, 138  
 Bavassano, B., Woo, R., & Bruno, R. 1997, *GeoRL*, **24**, 1655  
 Behannon, K. W., Neubauer, F. M., & Barnstorf, H. 1981, *JGR*, **86**, 3273  
 Bemporad, A. 2017, *ApJ*, **846**, 86  
 Bisi, M. 2016, in *Heliophysics: Active Stars, their Astrospheres, and Impacts on Planetary Environments*, ed. C. Schrijver, F. Bagenal, & J. Sojka (Cambridge: Cambridge Univ. Press), 289  
 Bisi, M. M., Jackson, B. V., Hick, P. P., et al. 2008, *JGR*, **113**, A00A11  
 Bravo, S., & Gonzalez-Esparza, J. A. 2000, *JGR*, **27**, 847  
 Bruno, R., Burlaga, L. F., & Hundhausen, A. J. 1982, *JGR*, **87**, 10339  
 Burger, R. A. 2012, *ApJ*, **760**, 60  
 Cohen, O. 2015, *SoPh*, **290**, 2245  
 Coppi, B., Laval, G., & Pellat, R. 1966, *PhRvL*, **16**, 1207  
 Crooker, N. U., Huang, C.-L., Lamassa, S. M., et al. 2004, *JGRA*, **109**, A03107  
 Czechowski, A., Strumik, M., Grygorczuk, J., et al. 2010, *A&A*, **516**, 10  
 Davis, L. 1965, in *Proc. IAU Symp. 22, Stellar and Solar Magnetic Fields*, ed. R. Lust (Amsterdam: North-Holland), 202  
 DeForest, C. E., Howard, R. A., Velli, M., Viall, N., & Vourlidas, A. 2018, *ApJ*, **862**, 18  
 DeRosa, M. L., Brun, A. S., & Hoeksema, J. T. 2012, *ApJ*, **757**, 96  
 Dobrowolny, M., & Trussoni, E. 1979, *NCimC*, **2**, 127  
 Drake, J. F., Swisdak, M., & Opher, M. 2015, *ApJL*, **808**, L44  
 Edmondson, J. K., Antiochos, S. K., DeVore, C. R., & Zurbuchen, T. H. 2010, *ApJ*, **718**, 72  
 Engelbrecht, N. E. 2019, *ApJ*, **872**, 124  
 Fisk, L. A. 1996, *JGR*, **101**, 15547  
 Girish, T. E., & Prabhakaran Nayar, S. R. 1988, *SoPh*, **116**, 369  
 Hale, G. E., Ellerman, F., Nicholson, S. B., & Joy, A. H. 1919, *ApJ*, **49**, 153  
 Heyvaerts, J., & Norman, C. 1989, *ApJ*, **347**, 1055  
 Higginson, A. K., Antiochos, S. K., DeVore, C. R., et al. 2017, *ApJL*, **840**, 1  
 Jackson, B. V., Bisi, M. M., Hick, P. P., et al. 2008, *JGR*, **113**, A00A15  
 Jackson, B. V., Buffington, A., Hick, P. P., et al. 2004, *SoPh*, **225**, 177  
 Jackson, B. V., Buffington, A., Hick, P. P., et al. 2006, *JGR*, **111**, A04S91  
 Jackson, B. V., Hick, P. P., Buffington, A., et al. 2009, *AnGeo*, **27**, 4097  
 Khabarova, O. V. 2013, *ARep*, **57**, 844  
 Khabarova, O. V., Malova, H. V., Kislov, R. A., et al. 2017a, *ApJ*, **836**, 108  
 Khabarova, O. V., & Obridko, V. N. 2012, *ApJ*, **761**, 82  
 Khabarova, O. V., Obridko, V. N., Kislov, R. A., et al. 2018, *PIPhR*, **44**, 840  
 Khabarova, O. V., Zank, G. P., Li, G., et al. 2015, *ApJ*, **808**, 181  
 Khabarova, O. V., Zank, G. P., Li, G., et al. 2016, *ApJ*, **827**, 122  
 Khabarova, O. V., Zank, G. P., Malandraki, O. E., et al. 2017b, *SunGe*, **12**, 23  
 Kislov, R. A., Khabarova, O. V., & Malova, H. V. 2015, *JGRA*, **120**, 8210  
 Korzhov, N. P. 1977, *SoPh*, **55**, 505  
 Lembege, B., & Pellat, R. 1982, *PhFl*, **25**, 1995  
 Maiewski, E. V., Kislov, R. A., Malova, H. V., et al. 2018, *PIPhR*, **44**, 80  
 Malova, H. V., Popov, V. Y., Grigorenko, E. E., et al. 2017, *ApJ*, **834**, 34  
 Malova, H. V., Popov, V. Y., Khabarova, O. V., et al. 2018, *CosRe*, **56**, 462  
 Mikić, Z., Linker, J. A., Schnack, D. D., et al. 1999, *PhPl*, **6**, 2217  
 Moss, D., Saar, S. H., & Sokoloff, D. D. 2008, *MNRAS*, **388**, 416  
 Mursula, K., & Hiltula, T. 2003, *GeoRL*, **30**, 2135  
 Nerney, S., Suess, S. T., & Schmahl, E. J. 1995, *JGR*, **100**, 3463  
 Ness, N. F., & Wilcox, J. M. 1964, *PhRvL*, **13**, 461  
 Obridko, V. N., Ivanov, E. V., Ozguc, A., et al. 2012, *SoPh*, **281**, 779  
 Obridko, V. N., & Shelting, B. D. 2008, *ARep*, **52**, 676  
 Osherovich, V. A., Fainberg, J., Fisher, R. R., et al. 1999, in *AIP Conf. 481, The Solar Wind Nine Conf.*, ed. S. R. Habbal (Woodbury, NY: AIP), 471  
 Osherovich, V. A., Tzur, I., & Gliner, E. B. 1984, *ApJ*, **284**, 412  
 Owens, M. J., & Lockwood, M. 2012, *JGRA*, **117**, A04102  
 Parker, E. N. 1958, *ApJ*, **128**, 664  
 Parker, E. N. 1969, *SSRv*, **9**, 325  
 Pizzella, G. 2018, *EPJC*, **78**, 848  
 Pizzo, V. J. 1982, *JGR*, **87**, 4374  
 Pneuman, G. W., & Kopp, R. A. 1971, *SoPh*, **18**, 259  
 Reville, V., Brun, A. S., Matt, S. P., et al. 2015, *ApJ*, **798**, 116  
 Sanderson, T. R., Appourchaux, T., Hoeksema, J. T., & Harvey, K. L. 2003, *JGRA*, **108**, 1035  
 Schatten, K. H., Wilcox, J. M., & Ness, N. F. 1969, *SoPh*, **6**, 442  
 Schultz, M. 1973, *Ap&SS*, **24**, 371  
 Schultz, M. 2007, in *AGU Fall Meeting, Conical Current Sheets in a Source-Surface Model of the Heliosphere* (Washington, DC: AGU), 1069  
 Schultz, M. 2008, in *AGU Fall Meeting, Non-Spherical Source-Surface Model of the Corona and Heliosphere for a Quadrupolar Main Field of the Sun* (Washington, DC: AGU), 4  
 Schwadron, N. A., & McComas, D. J. 2005, *GeoRL*, **32**, L03112  
 Simunac, K. D. C., Galvin, A. B., Farrugia, C. J., et al. 2012, *SoPh*, **281**, 423  
 Smith, C. W., & Bieber, J. W. 1991, *ApJ*, **370**, 435  
 Smith, E. J. 2001, *JGR*, **106**, 15819  
 Snodgrass, H. B. 1983, *ApJ*, **270**, 288  
 Sternal, O., Engelbrecht, N. E., Burger, R. A., et al. 2011, *ApJ*, **741**, 23  
 Suess, S. T., Ko, Y.-K., von Steiger, R., & Moore, R. L. 2009, *JGR*, **114**, A04103  
 Suess, S. T., McComas, D. J., Bame, S. J., & Goldstein, B. E. 1995, *JGR*, **100**, 12261  
 Svalgaard, L., & Wilcox, J. M. 1975, *SoPh*, **41**, 461  
 Svalgaard, L., Wilcox, J. M., & Duvall, T. L. 1974, *SoPh*, **37**, 157  
 Titov, V. S., Mikić, Z., Török, T., et al. 2012, *ApJ*, **759**, 70  
 Usmanov, A. V., & Goldstein, M. L. 2013, in *Numerical Modeling of Space Plasma Flows: ASTRONUM-2012*, Vol. 474 ed. N. V. Pogorelov, E. Audit, & G. P. Zank (San Francisco: ASP), 179  
 Usmanov, A. V., Goldstein, M. L., & Matthaeus, W. H. 2012, *ApJ*, **754**, 40  
 Veselovsky, I. S., Zhukov, A. N., & Panasenco, O. A. 2002, *SoSyR*, **36**, 80  
 Vlahakis, N., Tsinganos, K., Sauty, C., & Trussoni, E. 2000, *MNRAS*, **318**, 417  
 Wang, Y.-M. 2014, *SSRv*, **186**, 387  
 Wang, Y.-M., & Sheeley, N. R. 1990, *ApJ*, **355**, 726  
 Weber, E. J., & Davis, L., Jr. 1967, *ApJ*, **148**, 217  
 Wilcox, J. M. 1968, *SSRv*, **8**, 258  
 Wilcox, J. M., & Ness, N. F. 1965, *JGR*, **70**, 5793  
 Winterhalter, D., Smith, E. J., Burton, M. E., & McComas, D. J. 1994, *JGR*, **99**, 6667  
 Zelenyi, L. M., Artemyev, A. V., Malova, H. V., et al. 2008, *PhLA*, **372**, 6284